Fine structure of a biexciton in a single quantum dot with a magnetic impurity

Anna H. Trojnar,[1,2] Marek Korkusinski,[1] Udson C. Mendes,[1,3] Mateusz Goryca,[4] Maciej Koperski,[4] Tomasz Smolenski,[4] Piotr Kossacki,[4] Piotr Wojnar,[5] and Pawel Hawrylak[1,2]

[1]*Quantum Theory Group, Security and Disruptive Technologies Portfolio, Emerging Technologies Division, National Research Council, Ottawa K1A0R6, Canada*

[2]*Department of Physics, University of Ottawa, Ottawa, Canada*

[3]*Department of Physics of Condensed Matter, Institute of Physics "Gleb Wataghin", State University of Campinas, Campinas-SP, Brazil*

[4]*Institute of Experimental Physics, Faculty of Physics, University of Warsaw, Hoza 69, PL-00-681 Warsaw, Poland*

[5]*Institute of Physics, Polish Academy of Sciences, Warsaw, Poland*

(Received 28 February 2013; revised manuscript received 22 April 2013; published 28 May 2013)

We show theoretically and experimentally that the ground state of a biexciton in a CdTe self-assembled quantum dot with a magnetic Mn impurity exhibits a fine structure due to electron-electron Coulomb and electron-Mn exchange interactions. Results of exact diagonalization of the microscopic biexciton-manganese-ion model predict a pattern of three pairs of states in the ground-state manifold, each pair labeled by the projection of Mn spin. We show that the fine structure determines the ordering of the biexciton emission maxima and can be derived from the biexciton and exciton emission spectra. Theoretical predictions are successfully compared with measured biexciton and exciton emission spectra of a single CdTe dot with a Mn ion in its center.

DOI: 10.1103/PhysRevB.87.205311 PACS number(s): 78.67.Hc, 71.70.Gm, 78.55.Et

I. INTRODUCTION

The interaction of a localized spin with the spin of its environment is the basis of nuclear (NMR) and electron (EPR) spin-based imaging techniques widely applied in biology, medicine, and materials science.[1] However, when the electronic environment does not have a net spin, the localized spin does not interact with it directly except for the Kondo effect.[2,3] Here we show that spin-singlet few-electron systems such as pairs of holes or excitons confined in a quantum dot (QD)[4] do interact with a magnetic impurity, either a magnetic ion or a nuclear spin.[5–8] Such interactions are important for the imaging of the electronic system as well as the operation of electron spin-based qubits,[9] trions as intermediate state in optical spin manipulation,[10] entangled photon sources based on biexciton-exciton cascade,[11] operation of the quantum memory based on a single localized spin,[5,6,12] and nanomagnetism.[3,13–16]

The interaction of spin of electrons and holes in an exciton (X) confined in a QD and coupled to a magnetic impurity was analyzed experimentally[5,17–21] and theoretically.[22–26] In the following we show that it is possible for a localized spin to probe nonmagnetic, spin singlet, electronic environments. We realize the spin-singlet complex by optically injecting a biexciton (XX) into a single CdTe quantum dot containing a single manganese spin close to its center[5,17,18] [Fig. 1(a)]. Using a microscopic theory we predict and experimentally detect a fine structure of the XX coupled to the Mn^{2+} spin in a quantum dot. A preliminary detection of fine structure of XX interacting with the Mn^{2+} ion was reported in Ref. 17 and preliminary results of few-electron complexes coupled with Mn spin were reported in Refs. 12,25–28. The present work identifies the anisotropic Kondo-like coupling of the spin-singlet electronic system to the localized spin as responsible for the XX-Mn^{2+} fine structure.

This paper is organized as follows. Section I describes the microscopic model used to describe the XX-Mn^{2+} interactions. Section II presents simple analysis of a system of two holes and Mn^{2+}, while Sec. III expands this analytical analysis to XX-Mn^{2+} complex. Section IV discusses calculated emission spectra of XX-Mn^{2+} and compares them with the X-Mn^{2+} spectra, while Sec. V provides comparison of the calculated spectra to a measured ones. A summary is given in Sec. VI.

II. MODEL

In our microscopic approach[18,22] we approximate confining potential of the SAD by the two-dimensional anisotropic parabolic potential with the electron (hole) level spacing $\Omega_0^{e(h)}$. The single-particle (SP) states of this two-dimensional harmonic oscillator (HO), $|i\rangle = |n_+,n_-\rangle$, are enumerated by the HO quantum numbers n_+ and n_- and electron (heavy hole) spin projection $\sigma = \pm 1/2$, or $\uparrow,\downarrow$ ($\tau = \pm 3/2$, or $\Uparrow,\Downarrow$), respectively. Their energy $\varepsilon_i^{e(h)} = \Omega_0^{e(h)}(n_+ + n_- + 1)$. The SP states form shells (s, p, d,...) with increasing degeneracy.

In the first step of our analysis we consider an isotropic QD without the Mn^{2+} spin. The Hamiltonian of interacting confined carriers, written in the language of hole (electron) creation and annihilation operators $h_{i\tau}^+$ ($c_{i\sigma}^+$) and $h_{i\tau}$ ($c_{i\sigma}$) is $\hat{H}_{\rm EH} = \hat{T}_e + \hat{T}_h + \hat{V}_{\rm ee} + \hat{V}_{\rm hh} + \hat{V}_{\rm eh}$, where the electron kinetic energy $\hat{T}_e = \sum_{i,\sigma} \varepsilon_{i,\sigma}^e c_{i,\sigma}^+ c_{i,\sigma}$, the electron-electron interaction $\hat{V}_{\rm ee} = \sum_{ijkl,\sigma\sigma'} \langle i,j|V_{\rm ee}|k,l\rangle c_{i\sigma}^+ c_{j\sigma'}^+ c_{k\sigma'} c_{l\sigma}$, hole $\hat{T}_h$ and hole-hole operators $\hat{V}_{\rm hh}$ are analogous, and the electron-hole direct interaction is given by $\hat{V}_{\rm eh} = -\sum_{ijkl,\sigma\tau} \langle i,j|V_{\rm eh}|k,l\rangle c_{i\sigma}^+ h_{j\tau}^+ h_{k\tau} c_{l\sigma}$. $\hat{H}_{\rm EH}$ conserves the total angular momentum L of the carriers, and the total spin and spin projection of electrons (S, S_Z) and holes (J, J_Z). Denoting $\alpha = [L, J, J_Z, S, S_Z]$, in this step we diagonalize the electron-hole Hamiltonian $\hat{H}_{\rm EH}$ in the basis $|\alpha; ijkl\rangle$ of two-electron and two-hole configurations. This gives the energies E_r^α of N_α XX states, where $r = 1,\ldots,N_\alpha$. The corresponding eigenstates $|XX_r^\alpha\rangle = \sum_{ijkl}^{N_\alpha} A_{\alpha;ijkl}^{(r)} |\alpha; ijkl\rangle$ are linear combinations of two-pair configurations, in which single-particle orbitals i,j

(k,l) are occupied by holes (electrons) and $A^{(r)}_{\alpha;ijkl}$ are their amplitudes.

Next, we prepare the XX-Mn^{2+} basis as the tensor product $|XX^{\alpha}_r, M_Z\rangle = |XX^{\alpha}_r\rangle \otimes |M_Z\rangle$ of the XX eigenstates and the Mn^{2+} spin wave functions with $M_Z = \pm 5/2, \pm 3/2, \pm 1/2$. In this basis we construct and diagonalize the matrix of the Hamiltonian of the XX-Mn^{2+} system,[22] which takes the form $H_{\mathrm{XX-Mn}} = H_{\mathrm{EH}} + H_{\mathrm{EHX}} + H^{(e)}_{\mathrm{anis}} + H^{(h)}_{\mathrm{anis}} + H_{\mathrm{hMn}} + H_{\mathrm{eMn}}$. Here, $H_{\mathrm{EHX}} = \sum_{ijkl\sigma\sigma'\tau\tau'} \langle i\sigma, j\tau | V^{X}_{\mathrm{eh}} | k\tau', l\sigma'\rangle c^{+}_{i\sigma} h^{+}_{j\tau} h_{k\tau'} c_{l\sigma'}$ is the electron-hole exchange interaction.[30] $H^{(e)}_{\mathrm{anis}} = \sum_{ij\sigma} t^{e}_{ij} c^{+}_{i\sigma} c_{i\sigma}$ describes the anisotropy in the SP electron states, with t^{e}_{ij} proportional to the parameter $\gamma_e = (\Omega^2_{x,e} - \Omega^2_{y,e})/(\Omega^2_{x,e} + \Omega^2_{y,e})$ ($H^{(h)}_{\mathrm{anis}}$ is similar).[30] The ferromagnetic electron-Mn^{2+} spin interaction is described by the Heisenberg Hamiltonian,[8] $H_{\mathrm{eMn}} = -\sum_{i,j} \frac{J^{e}_{ij}}{2} [(c^{+}_{i\uparrow} c_{j\uparrow} - c^{+}_{i\downarrow} c_{j\downarrow}) M_Z + c^{+}_{i\downarrow} c_{j\uparrow} M^{+} + c^{+}_{i\uparrow} c_{j\downarrow} M^{-}]$, while the antiferromagnetic hole-Mn^{2+} Hamiltonian $H_{\mathrm{hMn}} = +\sum_{i,j} \frac{3J^{h}_{ij}(R)}{2} (h^{+}_{i\Uparrow} h_{j\Uparrow} - h^{+}_{i\Downarrow} h_{j\Downarrow}) M_Z$ is of Ising type, where M_Z is the projection of the Mn^{2+} spin, and J_{ij} is the orbital-dependent exchange constant.[12,18] Both exchange terms allow scattering of either particle between SP orbitals.[22] The amplitudes of this scattering are defined by the product of the respective SP wave functions: $J^{h(e)}_{ij}(R) = J^{h(e)}_{2\mathrm{D}} \Psi^{*h(e)}_{i}(R) \Psi^{h(e)}_{j}(R)$, where R is the position of the ion, and exchange constants $J^{h(e)}_{2\mathrm{D}} = J^{h(e)}_{3\mathrm{D}}/d$ are given by bulk exchange constants $J^{h(e)}_{3\mathrm{D}}$ and QD thickness d. Hole-Mn^{2+} scattering conserves the hole and Mn^{2+} spin, while the electron-Mn^{2+} Hamiltonian allows for spin flips. Having obtained the XX-Mn^{2+} eigenstates and energies we calculate its recombination spectra to the final states of X-Mn^{2+} using Fermi's golden rule.[22]

In numerical calculations the shell spacing is taken to be $\Omega_h + \Omega_e = 30$ meV, and $\Omega_e/\Omega_h = 4$. The e-Mn^{2+} and h-Mn^{2+} couplings $J^{h(e)}_{2\mathrm{D}} = 2J^{h(e)}_{(0)}/d$, where $J^{h}_{(0)} = 60$ meV nm^3 and $J^{e}_{(0)} = 15$ meV nm^3 with $d = 2$ nm being the height of the QD. Using bulk parameters and following Ref. 30 the short and anisotropic electron-hole exchange gives the bright-dark exciton splitting $\Delta_0 = 0.45$ meV, the bright exciton splitting $\Delta_1 = 0.16$ meV, and the dark exciton splitting $\Delta_2 = 0$. The energy is measured in effective Rydbergs ($\mathrm{Ry}^* = m^* e^4/2\varepsilon^2\hbar^2 = 13.4$ meV, where we use dielectric constant of the ZnTe barrier $\varepsilon = 7.4$).

III. SYSTEM OF TWO HOLES AND Mn^{2+}

To illustrate the effect of the coupling between a spin-singlet system and a localized magnetic moment, let us consider the localized Mn^{2+} spin $|\vec{M}| = 5/2$ interacting with a pair of holes confined in a QD. The ground-state configuration of two holes in a QD without the localized spin is a spin singlet $S = 0$ [Fig. 1(b)], and is created by placing the holes on the lowest-energy single-particle orbital $|0\rangle$: $|\mathrm{GS}\rangle = h^{+}_{0\Uparrow} h^{+}_{0\Downarrow} |v\rangle$, where $|v\rangle$ denotes the vacuum, and $h^{+}_{i\tau}$ ($h_{i\tau}$) creates (annihilates) a hole on the orbital i with spin τ.

Clearly, the expectation value $\langle M_Z | \langle \mathrm{GS} | H_{\mathrm{hMn}} | \mathrm{GS}\rangle | M_Z\rangle = 0$ for any M_Z, i.e., the holes and the Mn^{2+} spin are decoupled. Therefore, state $|\mathrm{GS}\rangle|M_Z\rangle$ is sixfold degenerate with energy E_{GS}, as shown schematically in the lower left-hand part of Fig. 1(d). As in the Kondo problem, Ref. 29, one can construct an excited triplet state $|\mathrm{ES}\rangle = \frac{1}{\sqrt{2}}(h^{+}_{1\Uparrow} h_{0\Uparrow} - h^{+}_{1\Downarrow} h_{0\Downarrow})|\mathrm{GS}\rangle$ by promoting a hole with either spin to the excited single-particle orbital $|1\rangle$ [Fig. 1(c)]. The $|\mathrm{ES}\rangle$ is decoupled from Mn^{2+}, which produces a sixfold degenerate excited manifold, with energy E_{ES}, represented in the upper left-hand part of Fig. 1(d).

The two degenerate manifolds, singlet and triplet, are coupled by the scattering term of hole-Mn Hamiltonian $H_{\mathrm{hMn}} \approx \frac{3}{2} J_{10} (h^{+}_{1\Uparrow} h_{0\Uparrow} - h^{+}_{1\Downarrow} h_{0\Downarrow}) M_Z$. The hole-$Mn^{2+}$ exchange interaction J_{10} scatters a hole from state $|0\rangle$ to state $|1\rangle$ in the effective magnetic field produced by the Mn^{2+} spin. We now evaluate the matrix element of the hole-Mn^{2+} interaction $\langle M_z | \langle \mathrm{GS} | H_{\mathrm{hMn}} | \mathrm{ES}\rangle | M_z\rangle$ between the ground and excited states for each Mn^{2+} spin projection:

$$\langle M_z | \langle \mathrm{GS} | \frac{3}{2} J_{10} (h^{+}_{1\Uparrow} h_{0\Uparrow} - h^{+}_{1\Downarrow} h_{0\Downarrow}) \hat{M}_Z \times \frac{1}{\sqrt{2}} (h^{+}_{1\Uparrow} h_{0\Uparrow} - h^{+}_{1\Downarrow} h_{0\Downarrow}) | \mathrm{GS}\rangle | M_z\rangle .$$

There are two minus signs, one in the Hamiltonian and one related to the Fermi statics (triplet character) of the excited state. They cancel each other and lead to the constructive interference resulting in $\langle M_z | \langle \mathrm{GS} | H_{\mathrm{hMn}} | \mathrm{ES}\rangle | M_z\rangle = \alpha M_z$, where $\alpha = 3J_{10}/\sqrt{2}$. With these off-diagonal matrix elements the sixfold degenerate ground-state manifold splits into three pairs of energy levels. The energy of each pair, $E_{-}(M_z) \approx E_{\mathrm{GS}} - \frac{\alpha^2}{E_{\mathrm{ES}} - E_{\mathrm{GS}}} |M_Z|^2$, acquires a correction proportional to $|M_Z|^2$, as shown in the right-hand side of Fig. 1(d). The excited manifold splits similarly, but with the reversed order of the gaps. This splitting depends on the form of h-Mn^{2+} exchange coupling—the splitting is largest for the Ising and vanishes for the isotropic Heisenberg coupling.[3] The results of numerical calculation of the XX fine structure described by the full microscopic Hamiltonian support this simple analysis.

IV. XX-MN^{2+} INTERACTION

Let us now discuss in detail how the Kondo-like coupling leads to pattern of XX-Mn^{2+} emission maxima. The singlet-singlet XX_{SS} correlated GS can be written as a linear combination of many configurations, of which the most important are

$$|XX_{\mathrm{SS}}\rangle = A^{\mathrm{SS}}_{\mathrm{ss\text{-}ss}} |s \Downarrow s \Uparrow, s \downarrow s\uparrow\rangle - A^{\mathrm{SS}}_{\mathrm{sd\text{-}ss}} (|s \Downarrow d \Uparrow, s \downarrow s\uparrow\rangle + |d \Downarrow s \Uparrow, s \downarrow s\uparrow\rangle). \quad (1)$$

The second configuration is created by promoting one hole to the $(1,1)$ state of the d shell of the QD. Note that the proper singlet antisymmetrization of this state requires the plus sign between the two configurations in the bracket.

The XX excited state XX_{TS} is built out of a triplet hole pair and is of the form

$$|XX_{\mathrm{TS}}\rangle = A^{\mathrm{TS}}_{\mathrm{sd\text{-}ss}} (|s \Downarrow d\Uparrow, s \downarrow s\uparrow\rangle - |d \Downarrow s\Uparrow, s \downarrow s\uparrow\rangle). \quad (2)$$

Here, the triplet state of two holes requires the minus sign between the two configurations. In this example the two electrons in the s shell form a singlet pair, and play a role

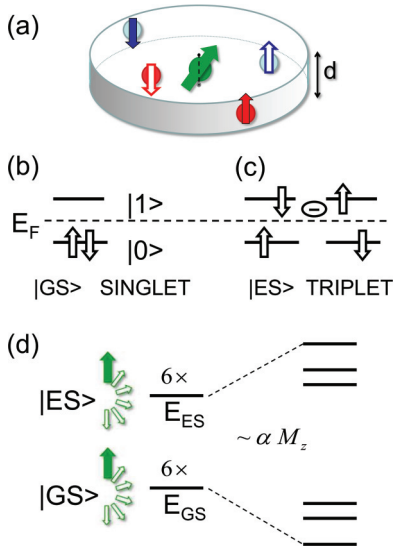

FIG. 1. (Color online) Schematic representation of the self-assembled quantum dot with a central Mn impurity interacting with two electron-hole pairs. (a) Mn impurity spin (green), the electron spins (solid arrows) and the hole spins (hollow arrows). (b) dominant two-hole singlet configuration in the $|\mathrm{GS}\rangle$, (c) dominant triplet configuration in the state $|\mathrm{ES}\rangle$. (d) Schematic energy diagram of the Mn two-hole complex—degenerate ground state and excited triplet manifold, interaction proportional to $|M_Z|$, and resulting splitting of both manifolds into three pairs (right).

of spectators. In numerical calculations all electrons and holes scatter and contribute to the ground and excited states. We can now identify the single-particle states appearing in the earlier analysis with the HO orbitals: the s-shell orbital (0,0) corresponds to the lower $|0\rangle$ state, and the d-shell orbital to the upper state $|1\rangle$ shown in Fig. 1. Therefore, we readily obtain the coupling of the first term of the singlet state $|XX_{\mathrm{SS}}\rangle \otimes |M_z\rangle$ with the triplet state $|XX_{\mathrm{TS}}\rangle \otimes |M_z\rangle$ as $\langle M_z|\langle XX_{\mathrm{SS}}|H_{\mathrm{hMn}}|XX_{\mathrm{TS}}\rangle|M_z\rangle = \alpha M_z$, where $\alpha = 3A^{\mathrm{SS}}_{\mathrm{ss\text{-}ss}}A^{\mathrm{TS}}_{\mathrm{ss\text{-}sd}}J^h_{\mathrm{sd}}$ is expressed in *microscopic* terms. Here, J^h_{sd} is the exchange constant describing the scattering from the s to the d orbital. Other contributions to the coupling, notably involving the second component of the $|XX_{\mathrm{SS}}\rangle$, are zero due to the central position of the Mn^{2+} spin in the QD (they play a role once the impurity is shifted from the center). As demonstrated previously, due to this coupling the sixfold degenerate ground XX-Mn^{2+} manifold splits into three pairs of states, with energies $E_-(M_z) = E_{\mathrm{SS}} - \frac{\alpha^2}{E_{\mathrm{TS}}-E_{\mathrm{SS}}}|M_z|^2$, corrected by a term proportional to the *magnitude* of $|M_z|$. The energy $E_-(M_z)$ is also dependent upon the splitting E_{TS}-E_{SS} of the energies of the excited and ground states of the bare XX. Final numerical results obtained by exact diagonalization of the full XX-Mn^{2+} Hamiltonian corroborrate results obtained by this simple model.

V. ANALYSIS OF EMISSION SPECTRA

Let us now explain how the interaction of XX with the Mn^{2+} ion can be observed in the XX emission spectrum. Without the Mn^{2+} mediated singlet-triplet coupling, the ground state of the XX is a product of the singlet state of

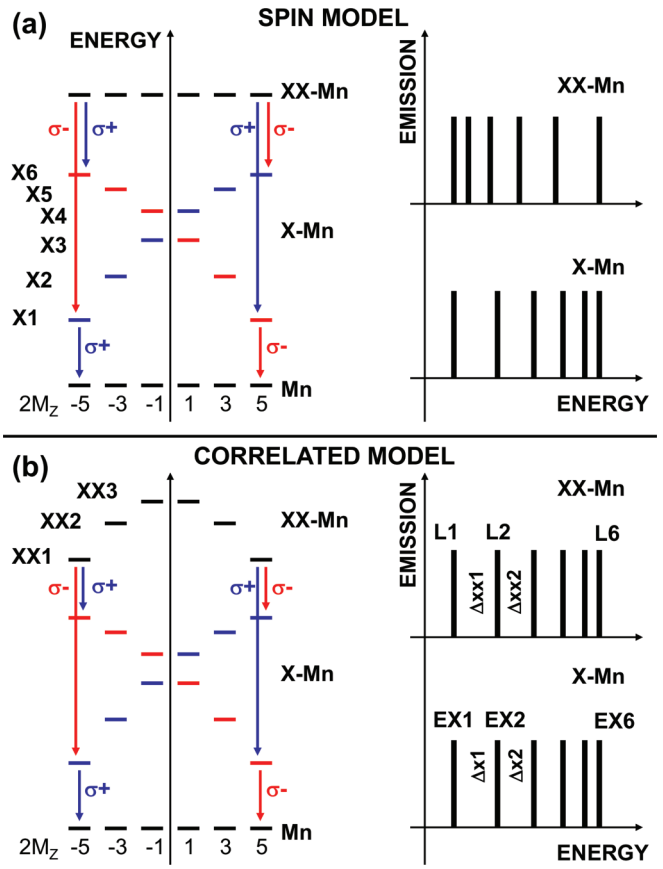

FIG. 2. (Color online) Left-hand diagrams show schematically the energies of the Mn, X-Mn^{2+} (bright subspace), and XX-Mn^{2+} systems in the spin model (a) and in the correlated model (b) as a function of the projection M_Z of the localized spin. Right-hand diagrams show the corresponding emission spectra. Gaps between X-Mn (XX-Mn^{2+}) lines are denoted as Δ_{Xi} (Δ_{XXi}).

holes and electrons, approximated for this discussion by the lowest-energy configuration $|XX_{\mathrm{SS}}\rangle = h^+_{s\Downarrow}h^+_{s\Uparrow}c^+_{s\downarrow}c^+_{s\uparrow}|v\rangle$, with electrons and holes distributed on the lowest single-particle state s, and the six states M_Z of the Mn^{2+} spin.[8] As already demonstrated for two holes, this XX-Mn^{2+} state is sixfold degenerate.

Figure 2(a) (left) shows schematically the energy alignment of the Mn^{2+}, X-Mn^{2+}, and XX-Mn^{2+} complexes in a diagram similar to that in Refs. 17,19. The Mn^{2+} and XX-Mn^{2+} states are plotted as a function of the M_Z (horizontal axis) as degenerate manifolds. The spectrum of X-Mn^{2+} complex built from the electron spin-down and hole spin-up states is shown in blue (opposite alignment in red). Note the irregular distribution of bright X-Mn^{2+} levels due to the quantum interference effect.[18,22] Emission from both X-Mn^{2+} and XX-Mn^{2+} occurs vertically within the same M_Z channel. The polarization of the resulting maxima is denoted by colors—blue (red) for $\sigma+$ ($\sigma-$). The right-hand side of this panel shows schematically the corresponding emission spectra: the XX-Mn^{2+} peaks are denser on the low-energy side of the spectrum, while the distribution of X-Mn^{2+} peaks is opposite.

Figure 2(b) illustrates the central result of this paper: the coupling of the XX complex with Mn^{2+} results in the splitting of the XX-Mn^{2+} sixfold degenerate manifold into three pairs.

The lowest-energy one, E_{XX1}, has $|M_z| = 5/2$, the higher, E_{XX2}, corresponds to $|M_z| = 3/2$, and the highest-energy E_{XX3} pair has $|M_z| = 1/2$. Each pair of levels is further split due to electronic spin flips, however this effect is not shown here. Similar splitting of XX-Mn levels was observed by Besombes *et al.*[17] who found that the injection of second exciton almost canceled the exchange interaction of X with Mn ion. The remaining splitting was attributed either to perturbation of the carrier orbital wave function by the Mn ion[17,28] or strain-induced magnetic anisotropy.[19] The predicted here splitting of energy levels of the XX-Mn^{2+} complex inverts the XX-Mn^{2+} emission spectrum compared to that in the single configuration case: now the pattern of gaps in the XX-Mn^{2+} and X-Mn^{2+} spectra is the same.

Let us now discuss emission spectra resulting from this arrangement of XX-Mn^{2+} levels. We use the notation introduced in Fig. 2(b) and consider the recombination channel with $M_z = -5/2$ as an example. Here, the XX-Mn^{2+} state has the lowest energy E_{XX1}. Since this state contains both $\sigma-$ and $\sigma+$ excitons, there are two recombination paths: (i) $\sigma+$ emission (blue), leaving the X-Mn^{2+} in the state $|h^+_{\Downarrow}c^+_{\uparrow}|v\rangle \otimes |-5/2\rangle$, and (ii) $\sigma-$ emission (red), with the final state $|h^+_{\Uparrow}c^+_{\downarrow}|v\rangle \otimes |-5/2\rangle$. The first event produces the lowest-energy emission line with energy $L_1 = E_{XX1} - E_{X6}$, while the second one produces the highest-energy line $L_6 = E_{XX1} - E_{X1}$. The same photon energies will be obtained in the channel $M_z = 5/2$, although with opposite polarizations, giving the unpolarized emission spectrum. The same procedure is applied to the other four XX-Mn^{2+} states to obtain the emission energies $L_2 - L_5$.

Figure 3(a) shows the XX-Mn^{2+} (red) and X-Mn^{2+} (black) emission spectra at $T = 75$ K, computed using fully microscopic Hamiltonian and exact diagonalization of the electron-hole-Mn^{2+} system.

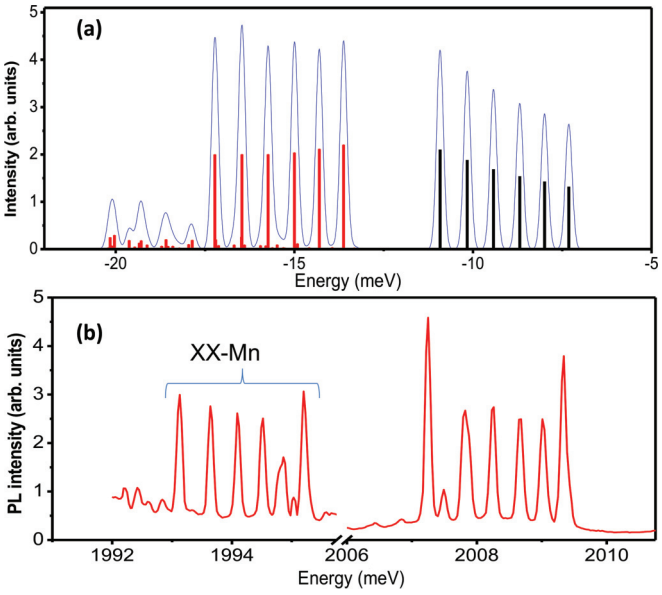

FIG. 3. (Color online) Computed (a) and measured (b) emission spectra of the QD, with the emission from X-Mn^{2+} complex (dashed black) and XX-Mn^{2+} complex (solid red) calculated for the temperature $T = 75$ K. In the calculated spectra energy is measured from the band gap energy of CdTe.

VI. EXPERIMENT AND DISCUSSION

Figure 3(b) shows the experimental spectra of the emission from quantum dots obtained for CdTe based heterostructures grown using molecular beam epitaxy. Each heterostructure contains a single layer of self-assembled CdTe QDs with a low concentration of Mn^{2+} ions, embedded in a ZnTe matrix. The density of quantum dots was about 5×10^9 cm^{-2}. The Mn^{2+} concentration was adjusted to obtain a significant number of QDs containing exactly one Mn^{2+} ion. For the measurement the sample was usually placed in the micro-photoluminescence setup composed of piezoelectric x-y-z stages and microscope lens. The system was kept in the superfluid helium assuring temperature about 2 K. The PL of the dots was excited either above the gap of the ZnTe barrier (at 532nm) or using tunable dye laser in the range 570–610 nm. The overall spatial resolution of the setup was better then 1 μm which assured possibility to select different single quantum dots containing a single Mn^{2+} ion. The PL analysis was done for the dots having emission lines in the low-energy tail of the broad PL emission band,[20] which assured good separation from the lines related to the other dots.

In Fig. 4 we analyze the gaps between the calculated (a) and measured (b)–(d) emission maxima. In Figs. 4(a)–4(d) we present the gaps measured in the average splitting Δ_{aver}. In Fig. 4(a), the calculated emission peak spacings for both X-Mn^{2+} (black dashed line)[18] and XX-Mn^{2+} (red solid line) typically decrease with increasing peak separation number i. Deviation from the linear decrease is due to the electron-hole exchange and anisotropy. We reemphasize that this tendency is opposite to that predicted by the spin model, where the peak spacing of XX-Mn^{2+} is a mirror image of that of X-Mn^{2+}

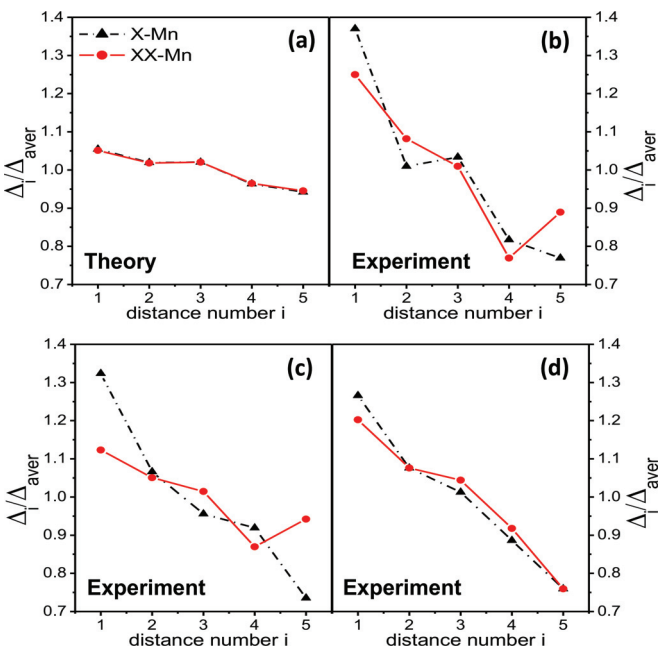

FIG. 4. (Color online) The normalized spacings of the emission lines (Δ_i/Δ_{aver}) of the X-Mn^{2+} (black) and XX-Mn^{2+} (red) (Δ_{aver} is average spacing), calculated (a) and extracted (b) from measured emission spectra shown in Figs. 3(a) and 3(b). (c) and (d) show different examples of the normalized spacings of the emission lines extracted from the measured emission spectra.

[see Fig. 2(a)]. The normalized spacings of the emission lines shown in Fig. 4(b) correspond to measured emission spectra shown in Fig. 3(b). All of the experimental results, presented in Figs. 4(b)–4(d), show the same trend as the calculated emission peak spacings [Fig. 3(a)].

In the X-Mn^{2+} emission spectra we have direct access to all energies E_{Xi}, as well as all XX-Mn^{2+} emission maxima L_i, as defined in Fig. 2(b). By extracting these values from our experimental spectra, we obtain the energy splitting of the XX-Mn^{2+} complex as shown in Fig. 1. The energies E_{XX1}, E_{XX2}, and E_{XX3} of the three groups are separated by: $\delta_2 = E_{XX2} - E_{XX1} = 0.2$ meV and $\delta_4 = E_{XX3} - E_{XX2} = 0.105$ meV. For comparison, our calculated splittings of the XX-Mn are $\delta_2 = 0.079$ meV and $\delta_4 = 0.039$ meV, close to the ones extracted from experiments by Besombes *et al.*[17] ($\delta_2 = 0.075$ meV and $\delta_4 = 0.035$ meV).

The fine structure of XX-Mn complex can also be detected directly by absorption of microwave radiation due to transitions in the Mn spin system as in NMR or EPR. The absorption of a photon requires change of angular momentum by one, with transitions of Mn spin from, e.g., $E_{-}(-5/2)$ to $E_{-}(-3/2)$ energy levels. The predicted absorbed photon energies would hence correspond to the two energy splittings, δ_2 and δ_4.

The model presented here is the simplest model capturing the essential physics of X- and XX-Mn complexes. To improve the theory a microscopic structure of a quantum dot, detailed understanding of confining potential for holes, degree of light-heavy hole mixing, and a fully atomistic model, as for III-V quantum dots,[31] might be required.

VII. SUMMARY AND OUTLOOK

In summary, we have shown that the localized Mn spin can couple to a nonmagnetic, spin-singlet state of biexciton by triplet excitations in analogy with perturbative approach to the Kondo effect. A microscopic model and exact diagonalization techniques lead to a pattern of three pairs of states in the ground-state XX manifold, each pair labeled by the projection of Mn^{2+} spin. The predicted fine structure in biexciton and exciton emission spectra is verified experimentally in a single CdTe quantum dot containing a manganese spin. The splitting of localized spin energy levels could potentially enable imaging of nonmagnetic molecular and solid-state systems as well as control of quantum devices based on electron and nuclear spin.

ACKNOWLEDGMENTS

The authors thank the Natural Sciences and Engineering Research Council of Canada (NSERC) and the Canadian Institute for Advanced Research for support. U.C.M also acknowledge CAPES-Brazil (Proc. 5860/11-3) and FAPESP-Brazil for financial support.

[1] R. J. Abraham, J. Fisher, and P. Loftus, *Introduction to NMR Spectroscopy* (Wiley, New York, 1988).
[2] J. Kondo, Prog. Theor. Phys. **32**, 37 (1964).
[3] A. Otte, M. Ternes, K. von Bergmann, S. Loth, H. Brune, C. Lutz, C. Hirjibehedin, and A. Heinrich, Nature Phys. **4**, 847 (2008).
[4] P. Hawrylak, and M. Korkusinski, in *Single Quantum Dots: Fundamentals, Applications, and New Concepts*, Topics in Applied Physics, Vol. 90, edited by P. Michler (Springer-Verlag, Berlin, 2003), p. 25.
[5] L. Besombes, Y. Leger, L. Maingault, D. Ferrand, H. Mariette, and J. CibertPhys. Rev. Lett. **93**, 207403 (2004).
[6] P. C. Maurer, G. Kucsko, C. Latta, L. Jiang, N. Y. Yao, S. D. Bennett, F. Pastawski, D. Hunger, N. Chisholm, M. Markham, D. J. Twitchen, J. I. Cirac, and M. D. Lukin, Science **336**, 1283 (2012).
[7] P. Hawrylak, in *Introduction to the Physics of Diluted Magnetic Semiconductors*, edited by J. Kossut and J. A. Gaj (Springer, Berlin, 2010.
[8] S.-J. Cheng and P. Hawrylak, Europhys. Lett. **81**, 37005 (2008).
[9] M. Korkusinski, P. Hawrylak, in *Semiconductor Quantum Bits.*, edited by F. Henneberger and O. Benson (Pan Stanford, Singapore, 2008.
[10] A. Greilich, S. E. Economou, S. Spatzek, D. R. Yakovlev, D. Reuter, A. D. Wieck, T. L. Reinecke, and M. Bayer, Nature Phys. **5**, 262 (2009).
[11] O. Benson, C. Santori, M. Pelton, and Y. Yamamoto, Phys. Rev. Lett. **84**, 2513 (2000).
[12] F. Qu and P. Hawrylak, Phys. Rev. Lett. **95**, 217206 (2005).
[13] F. Qu and P. Hawrylak, Phys. Rev. Lett. **96**, 157201 (2006).
[14] S. T. Ochsenbein, Y. Feng, K. M. Whitaker, E. Badaeva, W. K. Liu, X. Li, and D. R. Gamelin, Nature Nanotechnol. **4**, 681 (2009).
[15] R. M. Abolfath, M. Korkusinski, T. Brabec, and P. Hawrylak, Phys. Rev. Lett. **108**, 247203 (2012).
[16] Al. L. Efros, M. Rosen, and E. I. Rashba, Phys. Rev. Lett. **87**, 206601 (2001).
[17] L. Besombes, Y. Leger, L. Maingault, D. Ferrand, H. Mariette, and J. Cibert, Phys. Rev. B **71**, 161307(R) (2005).
[18] A. H. Trojnar, M. Korkusinski, E. S. Kadantsev, P. Hawrylak, M. Goryca, T. Kazimierczuk, P. Kossacki, P. Wojnar, and M. Potemski, Phys. Rev. Lett. **107**, 207403 (2011).
[19] C. Le Gall, A. Brunetti, H. Boukari, and L. Besombes, Phys. Rev. Lett. **107**, 057401 (2011).
[20] M. Goryca, T. Kazimierczuk, M. Nawrocki, A. Golnik, J. A. Gaj, P. Kossacki, P. Wojnar, and G. Karczewski, Phys. Rev. Lett. **103**, 087401 (2009).
[21] A. Kudelski, A. Lemaitre, A. Miard, P. Voisin, T. C. M. Graham, R. J. Warburton, and O. Krebs, Phys. Rev. Lett. **99**, 247209 (2007).
[22] A. H. Trojnar, M. Korkusinski, M. Potemski, and P. Hawrylak, Phys. Rev. B **85**, 165415 (2012).
[23] A. O. Govorov and A. V. Kalameitsev, Phys. Rev. B **71**, 035338 (2005).
[24] D. E. Reiter, T. Kuhn, and V. M. Axt, Phys. Rev. Lett. **102**, 177403 (2009).
[25] R. Oszwaldowski, P. Stano, A. G. Petukhov, and I. Zutic, Phys. Rev. B, **86**, 201408 (2012).
[26] J. Fernandez-Rossier, Phys. Rev. B **73**, 045301 (2006).
[27] N. T. T. Nguyen and F. M. Peeters, Phys. Rev. B **83**, 075419 (2011).

[28] J. Fernandez-Rossier, and R. Aquado, in *Handbook of spin transport and magnetism*, edited by E. Y. Tsymbal and I. Zutic (CRC Press, Boca Raton, 2011).
[29] E. S. Sorensen and I. Affleck, Phys. Rev. B **53**, 9153 (1996).
[30] A. H. Trojnar, E. S. Kadantsev, M. Korkusinski, and P. Hawrylak, Phys. Rev. B **84**, 245314 (2011).
[31] M. Zielinski, M. Korkusinski, and P. Hawrylak, Phys. Rev. B **81**, 085301 (2010).